Article

Modifying Electronic Communication in Dimolybdenum Units by Linkage Isomers of Bridged Oxamidate Dianions

F. Albert Cotton, Chun Y. Liu, Carlos A. Murillo, Dino Villagrn, and Xiaoping Wang

J. Am. Chem. Soc., **2003**, 125 (44), 13564-13575• DOI: 10.1021/ja036884e • Publication Date (Web): 14 October 2003

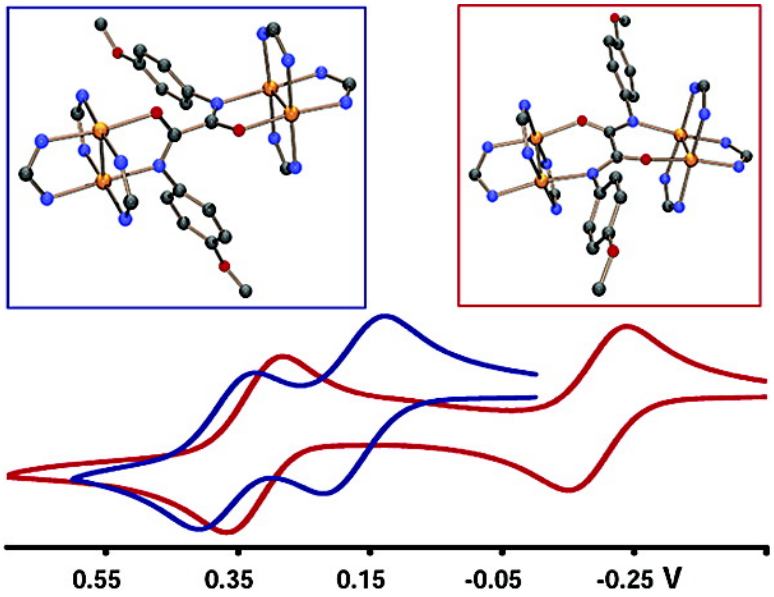

More About This Article

Additional resources and features associated with this article are available within the HTML version:

- Supporting Information
- Links to the 10 articles that cite this article, as of the time of this article download
- Access to high resolution figures
- Links to articles and content related to this article
- Copyright permission to reproduce figures and/or text from this article

View the Full Text HTML

J|A|C|S
ARTICLES
Published on Web 10/14/2003

Modifying Electronic Communication in Dimolybdenum Units by Linkage Isomers of Bridged Oxamidate Dianions

F. Albert Cotton,* Chun Y. Liu, Carlos A. Murillo,* Dino Villagrán, and Xiaoping Wang

Contribution from the Laboratory for Molecular Structure and Bonding, Department of Chemistry, P.O. Box 30012, Texas A&M University, College Station, Texas 77842-3012

Received June 24, 2003; E-mail: cotton@tamu.edu; murillo@tamu.edu

Abstract: Reactions of $Mo_2(O_2CCH_3)(DAniF)_3$, DAniF = *N*,*N*′-di-*p*-anisylformamidinate, with oxamidate dianions $[ArNC(O)C(O)NAr]^{2-}$, Ar = C_6H_5 and *p*-anisyl, give pairs of isomeric compounds where the $[Mo_2]$ units are bridged by the oxamidate anions. For the α isomers, the C−C unit of the dianion is nearly perpendicular to the Mo−Mo bonds, and these are essentially perpendicular to each other. For the β isomers, the corresponding C−C unit and the Mo−Mo bonds are essentially parallel to each other. Each type of isomer is stable in solution. The electronic communication as measured by the $\Delta E_{1/2}$ for the oxidation of each of the Mo_2 units is significantly better for the β isomers. This is supported also by the appearance of what is conventionally called an intervalence charge-transfer band in the near infrared region upon oxidation of the β isomers but not the α isomers. Molecular mechanics and DFT calculations help explain the relative conformations in the α isomers and the relative energy differences between the α and β isomers.

Introduction

The field of metal−metal bonded compounds encompasses a large number of interests because of their ability to act as catalysts,[1] their importance in medicine,[2] the study of electronic structure,[3] electronic communication,[4] and the fact that some are potent reducing agents that can be used in synthesis.[5] The most notable compounds are derivatives of the paddlewheel structure in which two metal atoms are spanned by four bridging ligands.[3] To date, two of the most important groups of ligands are the carboxylates and the amidinates such as formamidinates or benzamidinates that have two donor oxygen atoms for the former group and two nitrogen atoms in the latter group. Other kinds of ligands have a combination of *N* and *O* donor atoms. These comprise a variety of species such as carboxamidates, 2-hydroxypyridine (α-pyridone) derivatives, and others. The latter group has had a tremendous impact in the development of the chemistry of many elements especially that of singly bonded diplatinum compounds,[6] and they play a vital role in many of the widely studied *platinum blues*[7] which have chains of platinum atoms with formal oxidation numbers between +2 and +3.

In our laboratory, we have not only been studying compounds with a dimetal unit but have also focused our attention on linking such units with suitable equatorial and/or axial linkers with the purpose of forming extended supramolecular arrays varying from simple pairs to loops, triangles, squares, and other polygonal species.[8] These have been studied in many ways, but interest in the electronic communication between two units mediated by the nature of the linker has attracted a great deal

(1) (a) Doyle, M. P.; Ren, T. *Prog. Inorg. Chem.* **2001**, *49*, 113. (b) Estevan, F.; Herbest, K.; Lahuerta, P.; Barberis, M.; Pérez-Prieto, J. *Organometallics* **2001**, *20*, 950. (c) *Catalysis by Di- and Polynuclear Metal Cluster Complexes*; Adams, R. D., Cotton, F. A., Eds.; Wiley-VCH: New York, 1998. (d) Matsumoto, K. In *Cisplatin: Chemistry and Biochemistry of a Leading Anticancer Drug*; Lippert, B., Ed.; Wiley-VCH: New York, 1999; p 455. (e) Saeki, N.; Nakamura, N.; Ishibashi, T.; Arime, M.; Sekiya, H.; Ishihara, K.; Matsumoto, K. *J. Am. Chem. Soc.* **2003**, *125*, 3605. (f) Matsumoto, K.; Nagai, Y.; Matsunami, J.; Mizuno, K.; Abe, T.; Somazawa, R.; Kinoshita, J.; Shimura, H. *J. Am. Chem. Soc.* **1998**, *120*, 2900. (g) Doyle, M. P.; Forbes, D. C. *Chem, Rev.* **1998**, *98*, 911. (h) Doyle, M. P. In *Catalytic Asymmetric Synthesis*, 2nd ed.; Ojima, I., Ed.; Wiley-VCH: New York, 2000; Chapter 5.

(2) (a) Asara, J. M.; Hess, J. S.; Lozada, E.; Dunbar, K. R.; Allion, J. *J. Am. Chem. Soc.* **2000**, *122*, 8. (b) Catalan, K. V.; Hess J. S.; Maloney, M. M.; Mindiola, D. J.; Ward, D. L.; Dunbar, K. R. *Inorg. Chem.* **1999**, *38*, 3904. (c) Dale, L. D.; Dyson, T. M.; Tocher, D. A.; Tocher, J. H.; Edwards, D. I. *Anti-Cancer Drug Des.* **1989**, *4*, 295. (d) Aoki, K.; Yamazaki, H. *J. Chem. Soc., Chem. Commun.* **1980**, 186. (e) Howard, R. A.; Kimball, A. P.; Bear, J. L. *Cancer Res.* **1979**, *39*, 2568. (f) Fu, P.; Bradley, P. M.; Turro, C. *Inorg. Chem.* **2001**, *40*, 2476. (g) Aoki, K.; Salam, M. A. *Inorg. Chim. Acta* **2001**, *316*, 50. (h) Lippert, B. *Prog. Inorg. Chem.* **1989**, *37*, 1. (i) Micklitz, W.; Müller, G.; Huber, B.; Riede, J.; Rashwan, F.; Heinze, J.; Lippert, B. *J. Am. Chem. Soc.* **1988**, *110*, 7084.

(3) Cotton, F. A.; Walton, R. A. *Multiple Bonds between Metal Atoms*, 2nd ed.; Oxford University Press: Oxford, 1993.

(4) (a) Cotton, F. A.; Donahue, J. P.; Lin, C.; Murillo, C. A. *Inorg. Chem.* **2001**, *40*, 1234. (b) Cotton, F. A.; Donahue, J. P.; Murillo, C. A. *J. Am. Chem. Soc.* **2003**, *125*, 5436.

(5) (a) Cotton, F. A.; Daniels, L. M.; Murillo, C. A.; Timmons, D. J.; Wilkinson, C. C. *J. Am. Chem. Soc.* **2002**, *124*, 9249. (b) Cotton, F. A.; Gruhn, N. E.; Gu, J.; Huang, P.; Lichtenberger, D. L.; Murillo, C. A.; Van Dorn, L. O.; Wilkinson, C. C. *Science* **2002**, *298*, 1971.

(6) (a) Bandoli, G.; Dolmella, A.; Intini, F. P.; Pacifico, C.; Natile, G. *Inorg. Chim. Acta* **2003**, *346*, 143. (b) Dolmella, A.; Intini, F. P.; Pacifico, C.; Padovano, G.; Natile, G. *Polyhedron* **2002**, *21*, 275. (c) Zubavichus, Ya. V.; Slovokhotov, Yu. L.; Fedotova, T. N.; Kuznetsova, G. N.; Eremenko, I. L. *Russ. J. Inorg. Chem.* **2001**, *46*, 55. (d) Fedotova, T. N.; Minacheva, L. Kh.; Kuznetsova, G. N.; Sakharova, V. G.; Gel'fman, M. I.; Baranovskii, I. B.; *Russ. J. Inorg. Chem.* **1997**, *42*, 1838. (e) Fedotova, T. N.; Kuznetsova, G. N.; Korsunskii, V. I.; Baranovskii, I. B. *Russ. J. Inorg. Chem.* **1994**, *39*, 1284. (f) Fedotova, T. N.; Kuznetsova, G. N.; Minacheva, L. Kh.; Baranovskii, I. B. *Russ. J. Inorg. Chem.* **1993**, *38*, 84. (g) Korsunskii, V. I.; Kuznetsova, G. N. *Russ. J. Inorg. Chem.* **1988**, *33*, 923.

(7) (a) Matsumoto, K.; Sakai, K. *Adv. Inorg. Chem.* **2000**, *49*, 375. (b) Lippert, B. *Coord. Chem. Rev.* **1999**, *182*, 263. (c) O'Halloran T. V.; Lippard, S. J. *Isr. J. Chem.* **1985**, *25*, 130.

(8) (a) Cotton, F. A.; Lin, C.; Murillo, C. A. *Acc. Chem. Res.* **2001**, *34*, 759. (b) Cotton, F. A.; Lin, C.; Murillo, C. A. *Proc. Natl. Acad. Sci. U.S.A.* **2002**, *99*, 4810.

10.1021/ja036884e CCC: $25.00

of attention.[8] So far most efforts have been centered on using dicarboxylate linkers, although other types such as $M(OR)_4^{2-}$, M = S, Mo, W[9] and R = nothing or M = Co, Zn with R = CH_3 have also been examined.[10] One attempt at using diamidate (*N*, *O*) linkers to form pairs gave the appropriate product. However, the procedure had to be modified substantially from that used for making the analogous dicarboxylate analogues and many of the steps remained obscure, as reported in a preliminary communication for the ligands $ArNC(O)C_6H_4(O)CNAr$, Ar = C_6H_5 and $(m\text{-}CF_3)C_6H_4$.[11]

In the present report we further examine the linking of two dimetal units with diamidate anions which has led to the development of a new and what appears to be a general procedure of synthesis of compounds of this type. This employs as starting material the new compound $(CH_3COO)Mo_2(DAniF)_3$, **1** (DAniF = *N*,*N*′-di-*p*-anisylformamidinate), which contains a labile acetate anion and three much less labile formamidinate groups. As linkers we have used the oxamidate dianions $[ArNC(O)C(O)NAr]^{2-}$, Ar = C_6H_5 and *p*-anisyl, that have only a C−C bond instead of the C_6H_4 group between the amidate functionalities. The idea behind this change was that of improving electronic communication by shortening the distance between the two Mo_2 units.

Furthermore, these oxamidate anions, **I**, are structurally related to the simplest dicarboxylate dianion, namely, the oxalate anion, **II**, which has been so widely studied for the construction of supramolecular arrays[12] and for the study of magnetic properties of many such compounds (Chart 1).[13] These as well as the sulfur analogues, e.g., $[S_{2-n}O_nC-CS_{2-n}O_n]^{2-}$, n = 0, 1, have many known coordination modes[14] of which **III** is preferred for single metal dinuclear compounds. For such compounds we have found no report of type **IV** binding. For dimetal units united by linkers of this type, one could envision one of the two possible binding modes **V** or **VI**. A search of the Cambridge Crystallographic Data Base shows that there are only four compounds with paddlewheel-derived, metal−metal bonded units (M = Mo, Rh) and ligands of this type, all having the oxalate dianion[12b,15] and a handful of structurally characterized species having other dimetal units.[12d,e,16] Generally the

Chart 1

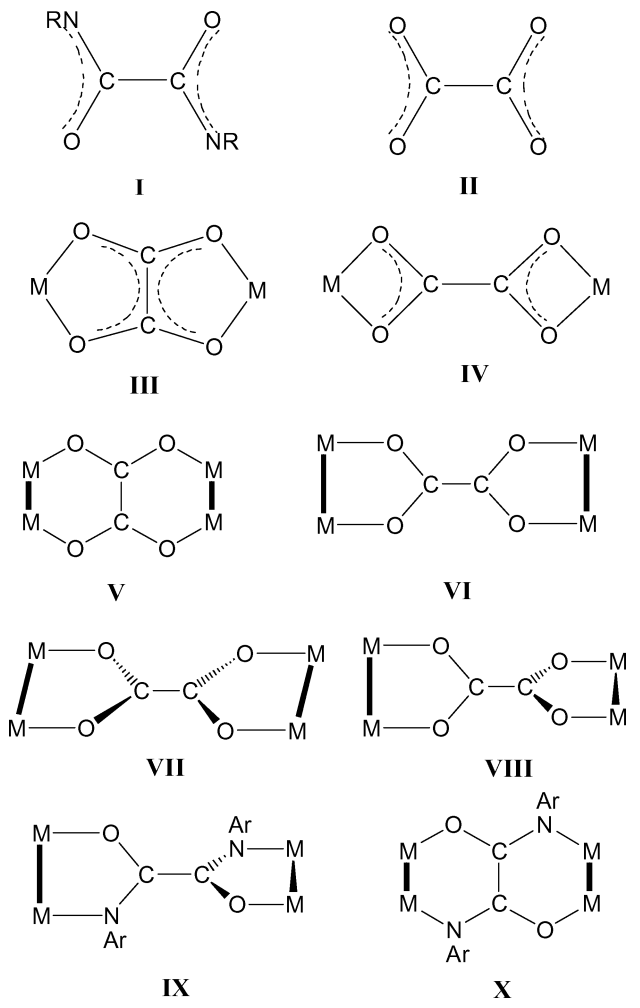

binding mode is of type **VI** where the two vectors of the metal−metal units are parallel but the vector of the C−C bond is perpendicular to the M−M bonds. In all cases, however, the O_2C-CO_2 unit is planar with D_{2h} symmetry, **VII**. Interestingly, theoretical calculations[17] for the isolated dioxalate anion have predicted that the more stable rotamer is the one with D_{2d} symmetry, **VIII**, instead of that with D_{2h} symmetry. Recently, oxalate salts having alkali metal ions have been examined by X-ray crystallography which shows that the oxalate ion can adopt either D_{2h} or D_{2d} conformations in the solid state.[18]

We now report the syntheses of four compounds with the formula $[Mo_2(DAniF)_3]_2$oxamidate (oxamidate = $[ArNC(O)C(O)NAr]^{2-}$, Ar = C_6H_5 and *p*-anisyl). For each of the Ar groups, two isomers were obtained and characterized structurally and otherwise, one set designated as the α isomers having a binding mode similar to **VI** but with each of the CON groups not in a planar conformation but almost perpendicular to each other as shown in **IX** and the other set referred to as the β isomers, **X**. For Ar = Ph, the α form is compound **2**; for Ar = anisyl, the corresponding complex is **3**. For the β isomers, the

(9) Cotton, F. A.; Donahue, J. P.; Murillo, C. A. *Inorg. Chem.* **2001**, *40*, 2229.
(10) Cotton, F. A.; Liu, C. Y.; Murillo, C. A.; Wang, X. *Inorg. Chem.* **2003**, *42*, 4619.
(11) Cotton, F. A.; Daniels, L. M.; Donahue, J. P.; Liu, C. Y.; Murillo, C. A. *Inorg. Chem.* **2002**, *41*, 1354.
(12) (a) Cotton, F. A.; Lin, C.; Murillo, C. A. *Chem. Commun.* **2001**, *11*. (b) Chisholm, M. H.; Wilson, P. J.; Woodward, P. M. *Chem. Commun.* **2002**, 566. (c) Lethbridge, Z. A. D.; Tiwary, S. K.; Harrison, A.; Lightfoot, P. *J. Chem. Soc., Dalton Trans*, **2001**, 1904. (d) Chen, Q.; Liu, S.; Zubieta, J. *Inorg. Chem.* **1989**, *28*, 4433. (e) Salignac, B.; Riedel, S.; Dolbecq, A.; Sécheresse, F.; Cadot, E. *J. Am. Chem. Soc.* **2000**, *122*, 10381. (f) Vaidhyanathan, R.; Natarajan, S.; Rao, C. N. R. *Chem. Mater.* **2001**, *13*, 3524. (g) Choudhury, A.; Natarajan, S. *Solid State Sci.* **2000**, *2*, 365. (h) Vaidhyanathan, R.; Neeraj, S.; Prasad, P. A.; Natarajan, S.; Rao, C. N. R. *Angew. Chem., Int. Ed.* **2000**, *39*, 3470. (i) Lethbridge, Z. A. D.; Lightfoot, P. *J. Solid State Chem.* **1999**, *143*, 58.
(13) (a) Vitoria, P.; Muga, I.; Gutiérrez-Zorrilla, J. M.; Luque, A.; Román, P.; Lezama, L.; Zúniga, F. J.; Beitia, J. I. *Inorg. Chem.* **2003**, *42*, 960. (b) Kahn, O. *Angew. Chem., Int. Ed. Engl.* **1985**, *24*, 834. (c) Julve, M.; Verdaguer, M.; Kahn, O.; Gleizes, A.; Philoche-Levisalles, O. *Inorg. Chem.* **1983**, *22*, 368. (d) Julve, M.; Verdaguer, M.; Kahn, O.; Gleizes, A.; Philoche-Levisalles, O. *Inorg. Chem.* **1984**, *23*, 3808. (e) Glerup, J.; Goodson, P. A.; Hodgson, D. J.; Michelsen, K. *Inorg. Chem.* **1995**, *34*, 6255.
(14) (a) Cotton, F. A.; Wilkinson, G.; Murillo, C. A.; Bochmann, M. *Advanced Inorganic Chemistry*, 6th ed.; John Wiley & Sons: New York, 1999; p 486. (b) Dietzsch, W.; Strauch, P.; Hoyer, E. *Coord. Chem. Rev.* **1992**, *121*, 43. (c) Mire, L. W.; Marynick, D. S. *Inorg. Chem.* **2000**, *39*, 5970.
(15) (a) Cotton, F. A.; Lin, C.; Murillo, C. A. *J. Chem. Soc., Dalton Trans.* **1998**, 3151. (b) Cotton, F. A.; Daniels, L. M.; Lin, C.; Murillo, C. A. *J. Am. Chem. Soc.* **1999**, *121*, 4538.
(16) (a) Johnson, B. F. G.; Lewis, J.; Raithby, P. R.; Saharan, V. P.; Wong, W. T. *Chem. Commun*, **1991**, 365. (b) Dolbecq, A.; Salignac, B.; Cadot, E.; Secheresse, F. *Bull. Pol. Acad. Sci. Chem.* **1998**, *46*, 237.
(17) (a) Dewar, M. J. S.; Zheng, Y.-J. *J. Mol. Struct. (THEOCHEM)* **1990**, *209*, 157. (b) Herbert, J. M.; Ortiz, J. V. *J. Phys. Chem.* A **2000**, *104*, 11786.
(18) Dinnebier, R. E.; Vensky, S.; Panthöfer, M.; Jansen, M. *Inorg. Chem.* **2003**, *42*, 1499.

corresponding compounds are designated as **4** and **5**. We also present molecular mechanics and density functional theory calculations that help explain the conformation and electronic structures of the α and β isomers.

Experimental Section

Materials and Methods. Solvents were freshly distilled under N_2 by employing standard procedures or dried and degassed using a Glass Contour solvent purification system. All synthetic operations were conducted under N_2 using Schlenk line techniques. $Mo_2(O_2CCH_3)_4$ was prepared by following a published method;[19] commercially available chemicals were used as received.

Physical Measurements. Elemental analyses were performed by Canadian Microanalytical Service, Delta, British Columbia, Canada. Electronic spectra in CH_2Cl_2 were measured in a range of 300 to 800 nm on a SHIMADZU UV-2501PC spectrophotometer and in the range of 800 to 3000 nm on a Cary 17 spectrophotometer. ^{1}H NMR spectra were recorded on a Mercury-300 NMR spectrometer with chemical shifts (δ ppm) referenced to $CDCl_3$ or DMSO-d_6. The electrochemical measurements were recorded at room temperature on a BAS 100 electrochemical analyzer with Pt working and auxiliary electrodes, Ag/AgCl reference electrode, scan rate of 100 mV/s, and 0.1 M Bu_4NPF_6 (in CH_2Cl_2) as electrolyte. Under these experimental conditions, the $E_{1/2}$ (Fc^+/Fc) was measured at 440 mV.

Preparation of $Mo_2(DAniF)_3(O_2CCH_3)$, 1. A mixture of yellow $Mo_2(O_2CCH_3)_4$ (1.43 g, 3.33 mmol) and *N*,*N*′-di-*p*-anisylformamidine (2.56 g, 10.00 mmol) was suspended in 100 mL of THF. While stirring, 20 mL of a 0.5 M solution of $NaOCH_3$ in methanol was added slowly. The color turned first to red and then to brown. The reaction was stirred for 5 h at room temperature, producing a deposit of white crystalline sodium acetate. After removal of the solvent under reduced pressure, the residue was extracted with ca. 40 mL of dichloromethane; filtration removed NaO_2CCH_3. The volume of the filtrate was then reduced to about 15 mL by vacuum evaporation. Ethanol (50 mL) was added to the residue with vigorous stirring. A yellow solid and a dark brown supernatant solution were obtained. After decanting, the solid was washed with ethanol (2 × 20 mL), followed by 20 mL of hexanes, and dried under vacuum. Yield: 2.83 g (84%). ^{1}H NMR (δ in $CDCl_3$): 8.50 (s, 2H, −NC*H*N−), 8.40 (s, 1H, −NC*H*N-), 6.67 (d, 8H, aromatic C−*H*), 6.50 (d, 8H, aromatic C−*H*), 6.45 (d, 4H, aromatic C−*H*), 6.24 (d, 4H, aromatic C−*H*), 3.72 (s, 12H, −OC*H*$_3$), 3.50 (s, 6H, −OC*H*$_3$), 2.61 (s, 3H, C*H*$_3$). UV−vis λ_{max} (nm) (ϵ, M^{-1} cm^{-1}): 439 (1.0×10^3). Anal. Calcd for $C_{47}H_{48}Mo_2N_6O_8$: C, 55.52; H, 4.76; N, 8.27. Found: C, 55.62; H, 4.74; N, 7.73.

Preparation of *N*,*N*′-Diphenyloxamide. A 500-mL flask containing a solution of oxalyl chloride, 8.00 g (63.0 mmol) in 100 mL of THF, was equipped with a dropping funnel. The flask was connected to a flask containing a saturated NaOH solution and cooled in an ice bath. With vigorous stirring, aniline (12.0 g, 129 mmol) was added dropwise to the solution of oxalyl chloride through the dropping funnel. A white solid was produced immediately, accompanied by a release of HCl which was absorbed by the NaOH solution. After the addition, the mixture was stirred for an additional half hour until heat release ceased. Then, 10 mL of H_2O was slowly added through the funnel, followed by addition of another 100 mL of H_2O. The precipitated white solid was collected by filtration, washed with H_2O, and dried overnight in air and then in a vacuum. Yield: 14.45 g (95%). ^{1}H NMR (δ, ppm in DMSO-d_6): 10.82 (s, 2H, N*H*), 7.86 (d, 4H, aromatic C*H*), 7.36 (t, 4H, aromatic C*H*), 7.14 (t, 2H, aromatic C*H*).

Preparation of *N*,*N*′-Di-*p*-anisyloxamide. A procedure similar to that just described was followed. With vigorous stirring, a solution of *p*-anisidine, 16.5 g (134 mmol) in 50 mL of THF, was added dropwise to a solution of oxalyl chloride, 8.33 g (65.7 mmol) in 100 mL of THF. This reaction produced a white solid of *N*,*N*′-dianisyloxamide. Yield: 18.0 g (91%). ^{1}H NMR (δ, ppm in DMSO-d_6): 10.70 (s, 2H, N*H*), 7.70 (d, 4H, aromatic C*H*), 6.94 (d, 4H, aromatic C*H*), 3.73 (s, 6H, OC*H*$_3$).

Preparation of α Isomers 2 and 3. The two compounds were synthesized similarly. To a stirred mixture of $Mo_2(DAniF)_3(O_2CCH_3)$ (0.410 g, 0.400 mmol) and *N*,*N*′-diphenyloxamide (0.050 g, 0.208 mmol) for **2**, or *N*,*N*′-di-*p*-anisyloxamide (0.062 g, 0.206 mmol) for **3**, in 25 mL of THF was added 1.5 mL of a 0.5 M solution of $NaOCH_3$ in methanol. An orange color developed immediately. The reaction mixture was stirred at room temperature for 3 h, and then the solvent was removed under vacuum. The orange residue was extracted with 15 mL of dichloromethane, and the mixture was passed through a filter frit packed with Celite to remove insoluble materials. The solvent from the filtered extract was removed under vacuum. Acetonitrile (20 mL) was added to the residue, producing a free-flowing, yellow solid. The mixture was stirred for 0.5 h; then the supernatant solution was decanted and the solid was washed with 15 mL of ethanol followed by 15 mL of hexanes and dried under vacuum. The crude product was dissolved in ca. 15 mL of dichloromethane; after filtration through a frit packed with Celite, hexanes (40 mL) were added to the filtrate to generate a yellow precipitate. Finally, the solid was collected by filtration and dried under vacuum. Yield of **2**: 0.320 g (75%). Yield of **3**: 0.340 g (78%). Crystals were obtained from CH_2Cl_2/hexane solutions. ^{1}H NMR (δ in $CDCl_3$) for **2**: 8.33 (s, 4H, −NC*H*N−), 8.25 (s, 2H, −NC*H*N−), 6.91 (t, 2H, aromatic C−*H*), 6.69 (d, 8H, aromatic C−*H*), 6.66 (d, 8H, aromatic C−*H*), 6.56 (d, 4H, aromatic C−*H*), 6.48 (d, 4H, aromatic C−*H*), 6.40 (d, 8H, aromatic C−*H*), 6.33 (d, 8H, aromatic C−*H*), 6.12 (d, 4H, aromatic C−*H*), 6.01 (d, 4H, aromatic C−*H*), 5.66 (d, 8H, aromatic C−*H*), 3.71 (s, 12H, −OC*H*$_3$), 3.66 (s, 12H, −OC*H*$_3$), 3.62 (s, 6H, −OC*H*$_3$), 3.60 (s, 6H, −OC*H*$_3$). ^{1}H NMR (δ in $CDCl_3$) for **3**: 8.38 (s, 4H, −NC*H*N−), 8.27 (s, 2H, −NC*H*N−), 6.71 (d, 8H, aromatic C−*H*), 6.69 (d, 8H, aromatic C−*H*), 6.42 (d, 16H, aromatic C−*H*), 6.34 (d, 4H, aromatic C−*H*), 6.18 (d, 4H, aromatic C−*H*), 6.10 (d, 4H, aromatic C−*H*), 6.04 (d, 4H, aromatic C−*H*), 5.76 (d, 8H, aromatic C−*H*), 3.74 (s, 12H, −OC*H*$_3$), 3.70 (s, 12H, −OC*H*$_3$), 3.65 (s, 6H, −OC*H*$_3$), 3.63 (s, 6H, −OC*H*$_3$), 3.60 (s, 6H, −OC*H*$_3$). UV−vis λ_{max} (nm) (ϵ, M^{-1} cm^{-1}) for **2**: 436 (2.0×10^3). UV−vis λ_{max} (nm) (ϵ, M^{-1} cm^{-1}) for **3**: 436 (1.8×10^3) Anal. Calcd for $C_{104}H_{100}Mo_4N_{14}O_{14}$ (**2**): C, 58.00; H, 4.68; N, 9.10. Found: C, 57.81; H, 4.58; N, 9.07. Anal. Calcd for $C_{106}H_{104}Mo_4N_{14}O_{14}$ (**3**): C, 58.35; H, 4.80; N, 8.99. Found: C, 58.14; H, 4.84; N, 8.68.

Preparation of β Isomers 4 and 5. A scale and procedure similar to the one described above was followed, but after removal of solvent in the first step, the residue was treated with hot ethanol (ca. 50 °C) instead of acetonitrile. Upon addition of the hot ethanol, a dark red solid formed immediately; the mixture was stirred at this temperature for half an hour and then cooled to room temperature. After the supernatant solution was decanted, the solid was washed with 15 mL of ethanol, followed by 15 mL of hexanes, and dried under vacuum. The red solid was dissolved in 15 mL of dicloromethane, and the solution was layered with 40 mL of hexanes. After diffusion over a period of 1 week, large dark-red crystals of the β isomer, along with yellow crystals of the corresponding α isomer, were formed. Manual separation from the mixture yielded 0.103 g (24%) of **4** and 0.113 g (26%) of **5**. ^{1}H NMR at 25 °C (δ in $CDCl_3$) for **4**: 6.62 (t, 2H, aromatic C−*H*), 6.57 (m, 4H, aromatic C−*H*), 6.41(d, 8H, aromatic C−*H*), 6.35−6.23 (m, 24H, aromatic C−*H*), 6.14 (d, 16H, aromatic C−*H*) 5.85 (d, 4H, aromatic C−*H*) 3.74 (s, 6H, −OC*H*$_3$), 3.69 (s, 12H, −OC*H*$_3$), 3.58 (s, 12H, −OC*H*$_3$), 3.51 (s, 6H, −OC*H*$_3$). At −50 °C: 8.57 (s, 4H, −NC*H*N−), 8.32 (s, 2H, −NC*H*N−), 6.60 (d, 4H, aromatic C−*H*), 6.52 (t, 2H, aromatic C−*H*), 6.42−6.27 (m, 32H, aromatic C−*H*), 6.12−6.03 (m, 16H, aromatic C−*H*), 5.86 (d, 4H, aromatic C−*H*), 3.75 (s, 6H, −OC*H*$_3$), 3.68 (s, 12H, −OC*H*$_3$), 3.57 (s, 12H, −OC*H*$_3$), 3.45 (s, 6H, −OC*H*$_3$). UV−vis λ_{max} (ϵ, M^{-1} cm^{-1}) for **4**: λ_{max}(1), 461 nm (2.0×10^3); λ_{max}(2), 541 nm (1.2×10^4). ^{1}H NMR at 25 °C (δ in $CDCl_3$) for **5**: 6.60 (d, 4H, aromatic C−*H*), 6.41 (d, 8H,

(19) Brignole, A. B.; Cotton, F. A. *Inorg. Synth.* **1972**, *13*, 87.

Table 1. X-ray Crystallographic Data for **1**, **3**, **4**, and **5**

	1	**3**·$2CH_2Cl_2$	**4**·$2CH_2Cl_2$	**5**·$2CH_2Cl_2$
empirical formula	$C_{47}H_{48}Mo_2N_6O_8$	$C_{108}H_{108}Cl_4Mo_4N_{14}O_{16}$	$C_{106}H_{104}Cl_4Mo_4N_{14}O_{14}$	$C_{108}H_{108}Cl_4Mo_4N_{14}O_{16}$
fw	1016.79	2383.64	2323.59	2383.64
space group	$P2_1/c$ (No. 14)	$C2/c$ (No. 15)	$C2/c$ (No. 15)	$C2/c$ (No. 15)
a, Å	9.938(1)	20.550(1)	30.813(2)	30.833(2)
b, Å	41.791(4)	18.990(1)	12.3766(8)	12.4356(8)
c, Å	10.887(1)	28.821(2)	28.069(2)	28.048(2)
β, deg	95.386(2)	105.400(1)	106.751(1)	100.423(1)
V, D^3	4501.5(8)	10843(1)	10250(1)	10577(1)
Z	4	4	4	4
T, K	213	213	213	213
λ, Å	0.7103	0.7103	0.7103	0.7103
d_{calcd}, g/cm^3	1.500	1.460	1.506	1.497
μ, mm^{-1}	0.617	0.620	0.653	0.636
R1[a] (wR2[b])	0.0728(0.1491)	0.088(0.185)	0.045(0.097)	0.049(0.088)

[a] $R1 = \Sigma||F_o| - |F_c||/\Sigma|F_o|$. [b] $wR2 = [\Sigma[w(F_o^2 - F_c^2)^2]/\Sigma[w(F_o^2)^2]]^{1/2}$.

aromatic C−*H*), 6.36 (b, d, 16H, aromatic C−*H*), 6.14 (d, 16H, aromatic C−*H*), 6.01 (b, 8H, aromatic C−*H*), 5.87 (d, 4H, aromatic C−*H*), 3.75 (s, 6H, −OCH_3), 3.68 (s, 12H, −OCH_3), 3.59 (s, 12H, −OCH_3), 3.55 (s, 6H, −OCH_3), 3.52 (s, 6H, −OCH_3). At −50 °C: 8.58 (s, 4H, −NC*H*N-), 8.36 (s, 2H, −NC*H*N−), 6.63 (d, 4H, aromatic C−*H*), 6.40 (b, 24H, aromatic C−*H*), 6.12 ∼ 6.02(m, 16H, aromatic C−*H*), 5.90 (b, m, 12H, aromatic C−*H*), 3.76 (s, 6H, −OCH_3), 3.67 (s, 12H, −OCH_3), 3.56 (s, 12H, −OCH_3), 3.50 (s, 12H, −OCH_3). UV−vis λ_{max} (ϵ, M^{-1} cm^{-1}) for **5**: λ_{max}(1), 461 nm (2.0×10^3); λ_{max}(2), 530 nm (1.2×10^4). Anal. Calcd for $C_{105}H_{102}Cl_2Mo_4N_{14}O_{14}$ (**4**·CH_2Cl_2): C, 56.66; H, 4.62; N, 8.80. Found: C, 56.71; H, 4.76; N, 8.70. Anal. Calcd for $C_{107}H_{106}Cl_2Mo_4N_{14}O_{14}$ (**5**·CH_2Cl_2): C, 57.00; H, 4.74; N, 8.70. Found: C, 57.20; H, 4.80; N, 8.79.

X-ray Structure Determinations. For each compound, a single crystal suitable for X-ray diffraction analysis was mounted on the tip of a quartz fiber with a small amount of silicone grease and attached to a goniometer head. Data for **1**, **3**·$2CH_2Cl_2$, **4**·$2CH_2Cl_2$, and **5**·$2CH_2Cl_2$ were collected at 213 K on a Bruker SMART 1000 CCD system equipped with a low-temperature controller cooled by liquid nitrogen. In each case, 20 frames were collected first to determine the orientation matrix. The cell parameters were calculated then through an auto-indexing routine and a hemisphere of data was collected. During the course of data collection, no crystal decay was observed. Data reduction and integration were performed with software package SAINT,[20] which corrects for Lorentz and polarization effects, while absorption corrections were applied by using the program SADABS.[21] Positions of non-hydrogen atoms were found by using the direct methods program in the Bruker SHELXTL software package.[22] Subsequent cycles of least-squares refinement followed by difference Fourier syntheses revealed the positions of remaining non-hydrogen atoms. Some of the anisyl group in the DAniF ligands and the interstitial CH_2HCl_2 molecules were found disordered in **3**·$2CH_2Cl_2$, **4**·$2CH_2Cl_2$, and **5**·$2CH_2Cl_2$, and they were refined with soft constraints. Hydrogen atoms were placed in calculated positions in final structure refinement. Crystal data and structural refinement information are in Table 1. Selected distances and angles are given in Table 2.

Computations. Molecular mechanics calculations were carried out using the software package Cerius[2] 4.6 by Accelrys.[23] Minimization and molecular mechanics calculations were performed with the Open Force Field (OFF) program, using the Universal Force Field.[24]

Table 2. Selected Bond Lengths (Å) and Angles (deg) for **3**, **4**, and **5**

	3·$2CH_2Cl_2$	**4**·$2CH_2Cl_2$	**5**·$2CH_2Cl_2$
Mo(1)−Mo(2)	2.0927(8)	2.0947(4)	2.0944(4)
Mo(1)−O(1)	2.123(5)		
Mo(1)−O(1A)		2.086(2)	2.093(2)
Mo(2)−N(1)	2.172(5)	2.202(2)	2.198(3)
Mo(1)−N(3)	2.127(6)	2.125(3)	2.147(3)
Mo(1)−N(5)	2.143(6)	2.118(3)	2.121(3)
Mo(1)−N(7)	2.128(6)	2.148(3)	2.133(3)
Mo(2)−N(2)	2.159(6)	2.169(3)	2.162(3)
Mo(2)−N(4)	2.165(6)	2.163(3)	2.161(3)
Mo(2)−N(6)	2.152(6)	2.159(3)	2.180(3)
Mo(1)−Mo(2)−N(1)	89.6(1)	98.60(6)	98.24(7)
Mo(2)−Mo(1)−O(1)	94.8(1)		
Mo(2)−Mo(1)−O(1A)		100.04(6)	100.31(6)

Geometric parameters from the single-crystal structure of **3** were used as the starting point for the simulation. Minimization of total energy was carried out by fixing the geometry of the $[N_8Mo_2](ON(Ar)C-CN(Ar)O)[Mo_2N_8]$ core and then varying the torsion angle defined by the O−C−C−O of the oxamidate from 85 to 195° using 5° incremental steps. In each case, all six anisyl groups from the formamidinate ligands and the aryl groups on the oxamidate bridge were unrestrained and allowed to rotate freely in the energy minimization process.

Density functional theory (DFT)[25] calculations were performed with the hybrid Becke-3[26] parameter exchange functional and the Lee−Yang−Parr[27] nonlocal correlation functional (B3LYP) implemented in the Gaussian 98 (Revision A.9) program suite.[28] Double-ζ quality basis sets (D95)[29] were used on nonmetal atoms (carbon, nitrogen, oxygen, and hydrogen). A small (1s2s2p3s3p3d) effective core potential (ECP) was used for the molybdenum atoms with a double-ζ basis set (LANL2DZ)[30] plus polarization functions.[31] Time-dependent density

(20) *SAINT. Data Reduction Software. Version 6.28A*; Bruker Analytical X-ray Systems, Inc.: Madison, WI, 2001.
(21) Sheldrick, G. M. *SHELXTL. Version 6.10*; Bruker Analytical X-ray Systems, Inc.: Madison, WI, 2000.
(22) *SADABS. Version 2.03, Area Detector Absorption and Other Corrections*. Bruker Advanced X-ray Solutions, Inc.: Madison, WI, 2002.
(23) Cerius[2] Forcefield-Based Simulations, Accelrys Inc.: San Diego, CA, 2001.
(24) (a) Rappe, A. K.; Casewit, C. J.; Colwell, K. S.; Goddard, W. A., III; Skiff, W. M. *J. Am. Chem. Soc*, **1992**, *114*, 10024. (b) Castonguay, L. A.; Rappe, A. K. *J. Am. Chem. Soc*. **1992**, *114*, 5832. (c) Rappe, A. K.; Colwell, K. S. *Inorg. Chem*. **1993**, *32*, 3438.
(25) (a) Hohenberg, P.; Kohn, W. *Phys. Rev*. **1964**, *136*, B864. (b) Parr, R. G.; Yang, W. *Density-Functional Theory of Atoms and Molecules*; Oxford University Press: Oxford, 1989.
(26) (a) Becke, A. D. *Phys. Rev. A* **1988**, *38*, 3098. (b) Becke, A. D. *J. Chem. Phys.* **1993**, *98*, 1372. (c) Becke, A. D. *J. Chem. Phys.* **1993**, *98*, 5648.
(27) Lee, C. T.; Yang, W. T.; Parr, R. G. *Phys. Rev. B* **1998**, *37*, 785.
(28) Frisch, M. J.; Trucks, G. W.; Schlegel, H. B.; Scuseria, G. E.; Robb, M. A.; Cheeseman, J. R.; Zakrzewski, V. G.; Montgomery, J. A.; Stratmann, R. E.; Burant, J. C.; Dapprich, S.; Millam, J. M.; Daniels, A. D.; Kudin, K. N.; Strain, M. C.; Farkas, O.; Tomasi, J.; Barone, V.; Cossi, M.; Cammi, R.; Mennucci, B.; Pomelli, C.; Adamo, C.; Clifford, S.; Ochterski, J.; Petersson, G. A.; Ayala, P. Y.; Cui, Q.; Morokuma, K.; Malick, D. K.; Rabuck, A. D.; Raghavachari, K.; Foresman, J. B.; Cioslowski, J.; Ortiz, J. V.; Stefanov, B. B.; Liu, G.; Liashenko, A.; Piskorz, P.; Komaromi, I.; Gomperts, R.; Martin, R. L.; Fox, D. J.; Keith, T.; Al-Laham, M. A.; Peng, C. Y.; Nanayakkara, A.; Gonzalez, C.; Challacombe, M.; Gill, P. M. W.; Johnson, B. G.; Chen, W.; Wong, M. W.; Andres, J. L.; Head-Gordon, M.; Replogle, E. S.; Pople, J. A. *Gaussian 98*, revision A.9; Gaussian, Inc.: Pittsburgh, PA, 1998.
(29) Dunning, T. H.; Hay, P. J. In *Modern Theoretical Chemistry*. 3. *Methods of Electronic Structure Theory*; Schaefer, H. F., III, Ed.; Plenum Press: New York, 1977; pp 1−28.

Scheme 1

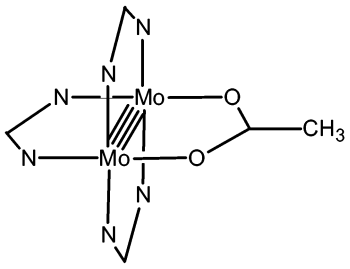

$Mo_2(DAniF)_3(O_2CCH_3)$

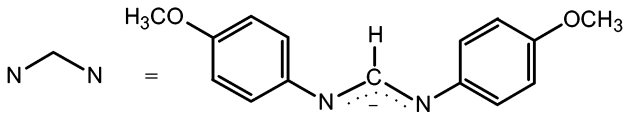

= *N*, *N*′-di(*p*-anisyl)formamidinate (DAniF)

functional (TD-DFT) calculations[32] were performed using the Gaussian program suite. All calculations were run on either an Origin 2000 32-processor or an Origin 3800 64-processor SGI computer located at the Texas A&M Supercomputing facility.

Results and Discussion

Precusor 1. We begin this section by discussing the properties of precursor **1** as this will set the basis for comparison with the oxamidate-bridged complexes **2**−**5**. The structure presented in the Supporting Information and shown in Scheme 1 is that of a paddlewheel in which three of the paddles are the formamidinate ligands while the fourth is an acetate group. Synthetically, this arrangement is important because the greater lability of the carboxylate group, relative to that of the formamidinate groups, allows subsequent substitution of only the former. This has been highlighted by the difficulties encountered by others in creating isolable extended arrays using only carboxylate ligands.[33] However, in our case, the lability of the carboxylate group becomes an advantage.

The Mo−Mo distance in **1** of 2.0892(8) Å is quite similar to those in the parents $Mo_2(DAniF)_4$[34] and $Mo_2(O_2CCH_3)_4$[35] which are 2.0964(5) and 2.0934(8) Å, respectively. The ^{1}H NMR spectrum in CD_3Cl is consistent with the arrangement about the dimetal unit having two singlets in the ratio of 2:1 for the two types of methine protons from the formamidinate ligands at δ values of 8.40 and 8.50 ppm. These are shifted downfield relative to those bound to nonmetal−metal bonded units because of the magnetic anisotropy of the quadruply bonded Mo_2 unit.[34,36] There are two singlets at 3.72 and 3.50 ppm which are also in the ratio of 2:1 that correspond to the methyl groups of the two types of *p*-anisyl groups in the formamidimate ligands and another singlet at 2.61 ppm from the methyl group of the acetate anion. The signals from the aromatic protons are in the range of 6.24 to 6.50 ppm. The electronic spectrum shows a strong band in the UV region corresponding to a LMCT transition and a weak band at 439 nm that can be assigned to the $\delta \rightharpoonup \delta^*$ transition.[3,37] The absorptions of the $\delta \rightharpoonup \delta^*$ transitions for $Mo_2(O_2CCH_3)_4$ and $Mo_2(DAniF)$ occur at 434 and 430 nm, respectively.[34,38] Finally, the cyclovoltammogram shows a reversible wave corresponding to a one-electron process at 292 mV. This value is between 465 mV for $Mo_2(O_2CCH_3)_4$ and 244 mV for $Mo_2(DAniF)_4$[34] measured under similar conditions.

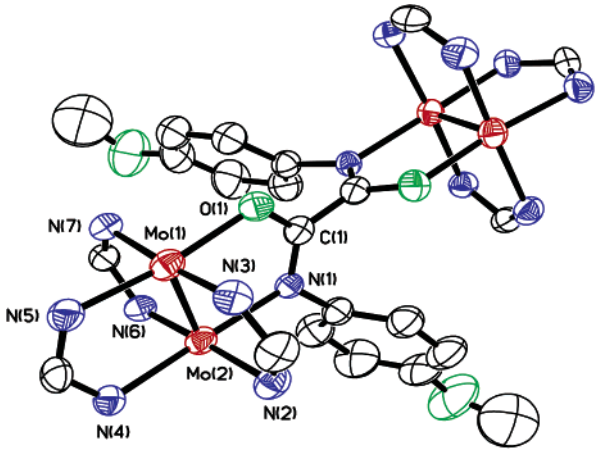

Figure 1. A view of the core of the α isomer in **3**·$2CH_2Cl_2$ showing the perpendicular arrangement of the two Mo−Mo units. Ellipsoids drawn at the 40% probability level. All *p*-anisyl groups on the formamidinate ions and hydrogen atoms have been omitted for clarity.

Structural Considerations for α and *β* Isomers. The structure of the α isomer **3** is shown in Figure 1. It has two $Mo_2(DAniF)_3$ units, which will be represented subsequently as [Mo_2], bridged by a dianisyloxamidate group. Compound **3** crystallizes in the space group *C*2/*c* with $Z = 4$. The Mo−Mo bond distance of 2.0927(8) Å falls within the narrow range for quadruply bonded units with similar ligand environments.[34] The C−C bond of the oxamidate anion is essentially perpendicular to the two Mo−Mo bonds as in the oxalate analogue.[4] However, unlike the oxalate analogue, the two Mo−Mo units are approximately perpendicular to one another instead of essentially parallel. The torsion angle between the two Mo_2 units is 81.6°. Thus, while the core structure of the oxalate analogue has idealized D_{2h} symmetry, the core of **3** has C_2 symmetry, which would be D_{2d} if not for the difference between the N and O atoms of the oxamide anion (as shown in Scheme 2). In other words, the C_{2h} and C_2 symmetries of the present compounds would be D_{2h} and D_2, respectively, for the oxalato-linked molecules. Tetranuclear dimolybdenum compounds [Mo_2]L[Mo_2] with two perpendicular [Mo_2] units have been seen only when tetrahedral linkers such as EO_4^{2-} (E = S, Mo, W) or $M(OCH_3)_4^{2-}$ (M = Zn, Co)[10,39] are employed or with the long

(30) (a) Wadt, W. R.; Hay, P. J. *J. Chem. Phys.* **1985**, *82*, 284. (b) Wadt, W. R.; Hay, P. J. *J. Chem. Phys.* **1985**, *82*, 299.
(31) Ehlers, A. W.; Böhme, M..; Dapprich, S.; Gobbi, A.; Höllwarth, A.; Jonas, V.; Köhler, K. F.; Stegmann, R.; Veldkamp, A.; Frenking, G. *Chem. Phys. Lett.* **1993**, *208*, 111.
(32) Casida, M. E.; Jamorski, C.; Casida, K. C.; Salahub, D. R. *J. Chem. Phys.* **1998**, *108*, 4439.
(33) (a) Cayton, R. H.; Chisholm, M. H.; Huffman, J. C.; Lobkovsky, E. B. *J. Am. Chem. Soc.* **1991**, *113*, 8709. (b) Bursten, B. E.; Chisholm, M. H.; Clark, R. J. H.; Firth, S.; Hadad, C. M.; MacIntosh, A. M.; Wilson, P. J.; Woodward, P. W.; Zaleski, H. M. *J. Am. Chem. Soc.* **2002**, *124*, 3050.
(34) Lin, C.; Protasiewicz, J. D.; Smith, E. T.; Ren, T. *Inorg. Chem.* **1996**, *35*, 6422.
(35) Cotton, F. A.; Mester, Z. C.; Webb, T. R. *Acta Crystallogr.* **1974**, *B30*, 2768.
(36) For a discussion of the magnetic anisotropy of metal−metal bonded species, see for example: (a) Cotton, F. A.; Daniels, L. M.; Lei, P.; Murillo, C. A.; Wang, X. *Inorg. Chem.* **2001**, *40*, 2778. (b) Cotton, F. A.; Daniels, L. M.; Murillo, C. A. *Angew. Chem., Int. Ed. Engl.* **1992**, *31*, 737. (c) Cotton, F. A.; Ren, T. *J. Am. Chem. Soc.* **1992**, *114*, 2237. (d) Cotton, F. A.; Kitagawa, S. *Polyhedron* **1988**, *18*, 1673.
(37) Cotton, F. A.; Nocera, D. G. *Acc. Chem. Res.* **2000**, *33*, 483.
(38) Liwporncharoenvong, T.; Luck, R. L. *J. Am. Chem. Soc.* **2001**, *123*, 3615.

Scheme 2

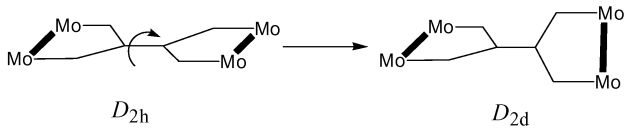

allene-1,3-dicarboxylate linker.[4b] As we shall see later, the molecular geometry of the α isomers can be attributed to the steric effect resulting from the bulky *p*-anisyl groups on the oxamidate anion.

Crystals of **2** have been made also, and like **3**, **2** crystallizes in the monoclinic space group *C*2/c, with the molecule residing on a crystallographic special position of C_2 symmetry.[40] Unfortunately, severe crystallographic disorder has prevented full structural refinement. Indeed, this was the initial reason for studying **3**. However, the data provided unequivocal evidence of the structure. Compounds **2** and **3** have similar cores with the two [Mo$_2$] units in a gauche conformation. Further evidence of the structural similarity of **2** and **3** comes from the ^{1}H NMR and UV−vis spectra (vide infra).

As shown in Figures 2 and 3, the core structures of the two *β* isomers, **4** and **5**, are quite different from those of the α isomers. The most striking difference is that in these isomers the diaryloxamidate anions chelate the two [Mo$_2$] units, giving two six-membered rings formed by the Mo−Mo−N−C−C−O groups. Therefore, unlike the α isomers, the two Mo−Mo units and the central C−C bond are nearly parallel. This coordination mode is common for compounds having the parent oxalate ligands in binuclear complexes with single transition metal atoms where the unit that includes the metal atoms is a five-membered ring. The six-atom rings are not strictly coplanar, and the overall structure is slightly bent (Figures 2 and 3). However, the Mo−Mo bond distances of 2.0947(4) and 2.0945(4) Å for the *β* forms **4** and **5** are essentially the same as those for the α isomers **2** and **3** and in the precursor **1**. The difference in the conformation of the oxamidate groups in the α and *β* isomers does not appear to influence the central C−C bond distances either as these are 1.50(1), 1.519(6), and 1.526(6) Å for **3**, **4**, and **5**, respectively. It should be noted that some of the theoretical calculations on the oxalate anion noted earlier had predicted a slight increase of 0.01−0.02 Å[33b] in C−C distances in changing from the orthogonal to the planar form.

Spectroscopy of the α and *β* Isomers. For **2**, **3**, **4**, and **5**, the colors differ greatly from one type of isomer to the other; the α isomers (**2** and **3**) are yellow color, whereas the *β* isomers are wine-red. Consistent with the differences in the color, it is observed that the electronic spectra in the visible region for the two isomeric forms are quite different. Figure 4 shows the absorption spectra in the visible region of both α and *β* isomers, represented by **2** and **4**, respectively. Only these two are shown as the spectra of the other two compounds of the same isomeric forms are essentially identical. For **2** and **3**, there is no low energy absorption observed and the shoulder at $\lambda_{max} = 436$ nm (ϵ, 2.0×10^3 M^{-1} cm^{-1}), which is similar to that of **1**, can be assigned unambiguously to the $\delta \rightarrow \delta^*$ transition. The $\delta \rightarrow \delta^*$ transition has been well established from the studies of a variety of paddlewheel, quadruply bonded dimolybdenum compounds. In previous studies, it has been found that for [Mo$_2$]L[Mo$_2$] compounds with a conjugated tetradentate ligand L, a $\delta \rightarrow \pi^*$

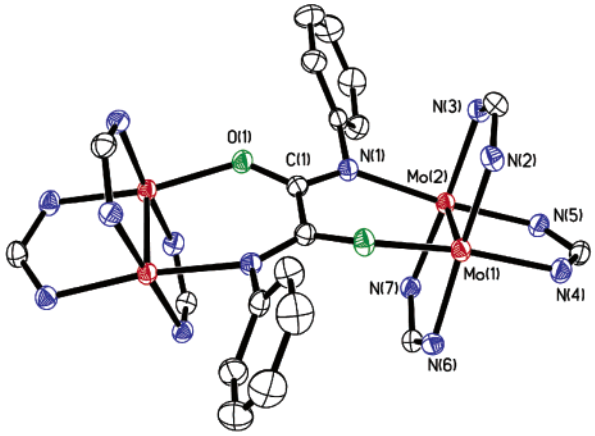

Figure 2. A view of the core of the *β* isomer in **4**·2CH$_2$Cl$_2$ showing the almost parallel arrangement of the two Mo−Mo units and C−C bond of the oxamidate bridge. Displacement ellipsoids are drawn at the 40% probability level. All *p*-anisyl groups on the formamidinate ions and hydrogen atoms have been omitted for clarity.

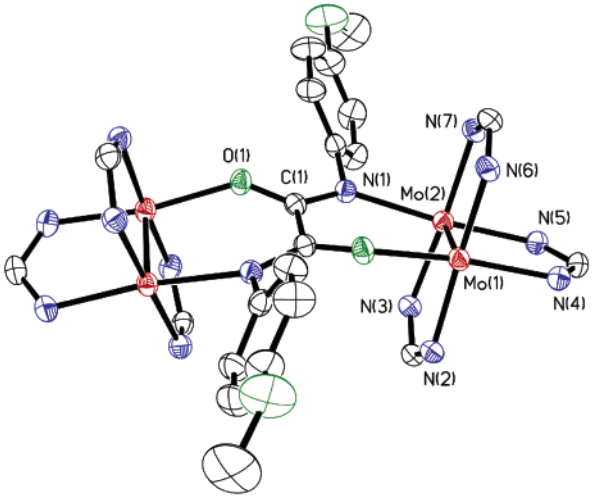

Figure 3. A view of the core of **5** in **5**·2CH$_2$Cl$_2$ drawn with 40% probability elliposoids. All *p*-anisyl groups on the formamidinate ions and hydrogen atoms have been omitted for clarity.

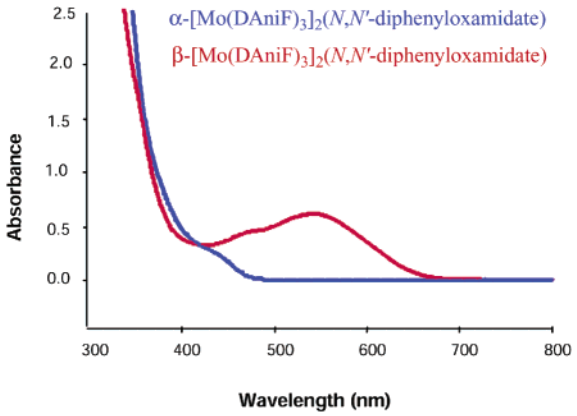

Figure 4. Electronic spectra of α [Mo$_2$(DAniF)$_3$]$_2$(*N*,*N*′-diphenyloxamidate), **2**, and *β* [Mo$_2$(DAniF)$_3$]$_2$(*N*,*N*′-diphenyloxamidate), **4**, in CH$_2$Cl$_2$ solution. The spectra of **3** and **5** are similar to those of **2** and **4**, respectively.

(39) It should be noted that compounds with L = M(OCH$_3$)$_4^{2-}$ have been oxidized recently. See: Cotton, F. A.; Dalal, N. S.; Liu, C. Y.; Murillo, C. A.; North, J. M.; Wang, W. *J. Am. Chem. Soc.* In press.

(40) Crystal data for **2**·2CH$_2$Cl$_2$: $C_{106}H_{104}Cl_4Mo_4N_{14}O_{14}$, $M = 2323.59$, monoclinic, space group *C*2/*c*, $a = 20.157(2)$ Å, $b = 18.743(2)$ Å, $c = 28.626(3)$ Å, $\beta = 106.178°$, $Z = 4$, $V = 10387(2)$ Å^3.

transition (MLCT) dominates the electronic spectra in the visible region.[41] This is a consequence of the interaction between the δ orbital of the $[Mo_2]$ units and the π orbital of the linker by which the ligand-based π^* orbital is energetically lowered relative to that of the metal-based δ^*. Obviously, this is not what is observed for the α isomers **2** and **3**. The interaction of the δ orbital from the $[Mo_2]$ units with the linker π^* orbital is minimized because of the two orthogonal CNO groups in the oxamidate anion. Thus, the two linked $[Mo_2]$ units behave as two independent, uncoupled dimetal species. This is why the spectroscopic properties of **2** and **3** are so similar to those with simple paddlewheel Mo_2^{4+} units such as **1** but significantly different from those of the oxalate analogue and those of the β forms where the oxamidate anion is planar, allowing more electronic communication between Mo_2 units.

Compounds **4** and **5** (β isomers) present electronic spectra with two well-resolved absorption bands in the visible region (Figure 4). The one of lower intensity at higher energy (λ_{max} = 461 nm, $\epsilon = 2.0 \times 10^3$ M^{-1} cm^{-1}) can be reasonably assigned as the $\delta \rightarrow \delta^*$ transition, as discussed above. The intense absorptions at lower energy, λ_{max} 541 nm (ϵ, 1.2×10^4 M^{-1} cm^{-1}) for **4** and λ_{max} 530 nm (ϵ, 1.2×10^4 M^{-1} cm^{-1}) for **5**, are responsible for the wine-red color of the β isomers and can be assigned to an MLCT $\delta \rightarrow \pi^*$ transition. The orbital interactions involving $[Mo_2]$ units (δ) and the oxamidate anion (π) are optimized in the planar environment. Furthermore, the distances of 6.322 and 6.334 Å between the two $[Mo_2]$ units in **4** and **5** are significantly shorter than those in **2** and **3**. Therefore the $\delta \rightarrow \pi^*$ back-bonding in this system is stronger than that for of the dicarboxylate-linked analogues and it is consistent with the electrochemical behavior presented later.

For the two α isomers, the room-temperature ^1H NMR spectra are consistent with the structure of the molecules, with all signals having the expected chemical shifts (ppm) and relative intensities. The well-documented[34,36] singlets for the methine protons appear at 8.38 ppm (4 H) and 8.27 ppm (2 H). The downfield shifts are due to the deshielding effect caused by the magnetic anisotropy of the Mo−Mo quadruple bond.[36] For compounds of the type $[Mo_2]L[Mo_2]$ (L = tetradentate ligand), a ratio of 2:1 for the methine protons is expected because there are four *cis* and two *trans* coordinated formamidinate anions surrounding the two $[Mo_2]$ units and indeed this is observed for the α isomers.

Interestingly, the room-temperature ^1H NMR spectra in $CDCl_3$ for the two β isomers do not show the expected signals for methine protons in the region of 8−9 ppm, but upon cooling to −40 °C, two peaks in a ratio of 2:1 appear at 8.5 and 8.2 ppm which is consistent with the solid-state structure.[42] Importantly, the different behavior of the α and β isomers in the NMR studies indicates that once formed each of the isomers is stable in solution and there is no detectable interconversion.

Electrochemistry. All four compounds display two reversible one-electron redox waves ($E_{1/2}^{+1/0}$ and $E_{1/2}^{+2/+1}$), which correspond to two successive redox processes occurring at each of the two dimetal units as described by Scheme 3. Electrochemical data for **2**, **3**, **4**, and **5** at room temperature, along with calculated comproportionation constants, K_c, are listed in Table 3. For comparison, the results of electrochemical measurements of some relevant compounds are given.

Scheme 3

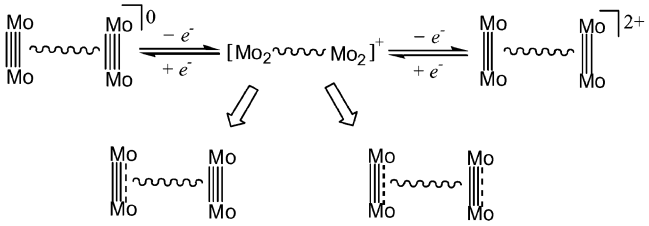

localized, Class I delocalized, Class III

Table 3. Oxidation Potentials and Comproportionation Constants for Some $[Mo_2]$(linker)$[Mo_2]$ Compounds

linker	$E_{1/2}(1)$, mV	$E_{1/2}(2)$, mV	$\Delta E_{1/2}$, mV	K_c	ref
α-diphenyloxamidate (**2**)	176	367	191	1.7×10^3	this work
α-di-*p*-anisyloxamidate (**3**)	183	373	190	1.6×10^3	this work
β-diphenyloxamidate (**4**)	−157	383	540	1.3×10^9	this work
β-di-*p*-anisyloxamidate (**5**)	−196	327	523	6.9×10^8	this work
oxalate	294	506	212	3.8×10^3	4b
$Zn(OMe)_4^{2-}$	−208	4	212	3.8×10^3	10,39
$Co(OMe)_4^{2-}$	−211	−4	207	3.2×10^3	10,39
SO_4^{2-}	93	321	228	7×10^3	9

The electrochemical behavior for the two α isomers, **2** and **3**, and the two β isomers, **4** and **5**, is qualitatively similar for the isomers of each type but very different from one isomer to another. The $E_{1/2}$s for the approximately planar β isomers are shifted to more negative values relative to those of the α isomers and the oxalate analogue, which indicates that the β isomers should be good candidates for chemical oxidation. In Figure 5, cyclic voltammograms (CV) and differential pulse voltammograms (DPV) for **3** and **5** are plotted. It is clear that the separation between the two peaks is quite different with the β isomers showing a significantly larger separation ($\Delta E_{1/2}$) than for the α isomers. This shows in a very direct way that there is a great difference between one type of isomer and the other in terms of electronic communication, as was indicated by results from electronic and NMR spectra discussed above.

Similar to binuclear complexes with two redox sites, a constant for the comproportionation equilibrium involving species at three different oxidation levels can be derived from the separation of potentials between the two redox couples ($\Delta E_{1/2}$).[43] The comproportionation constant, K_c, which is exponentially related to $\Delta E_{1/2}$, measures the thermodynamic stability of the mixed-valence species, formally $[Mo_2^{5+}]L[Mo_2^{4+}]$.

$$[Mo_2^{5+}]L[Mo_2^{5+}] + [Mo_2^{4+}]L[Mo_2^{4+}] \rightleftharpoons 2[Mo_2^{5+}]L[Mo_2^{4+}] \quad K_c$$

$$K_c = e^{\Delta E_{1/2}/25.69}$$

This to some extent must reflect the degree of electron delocalization between the two dimetal centers. It has been established by the studies in both single-metal binuclear systems and dimetal, tetranuclear systems that two major factors influence the value of the comproportionation constant K_c.[41,44]

(41) Cotton, F. A.; Donahue, J. P.; Murillo, C. A.; Pérez, L. M. *J. Am. Chem. Soc.* **2003**, *125*, 5486.
(42) We are currently synthesizing other oxamidate derivatives and studying the dynamic processes in detail.
(43) Richardson, D. E.; Taube, H. *Inorg. Chem.* **1981**, *20*, 1278.
(44) (a) Creutz, C. *Prog. Inorg. Chem.* **1983**, *30*, 1. (b) Richardson, D. E.; Taube, H. *Coord. Chem. Rev.* **1984**, *60*, 107.

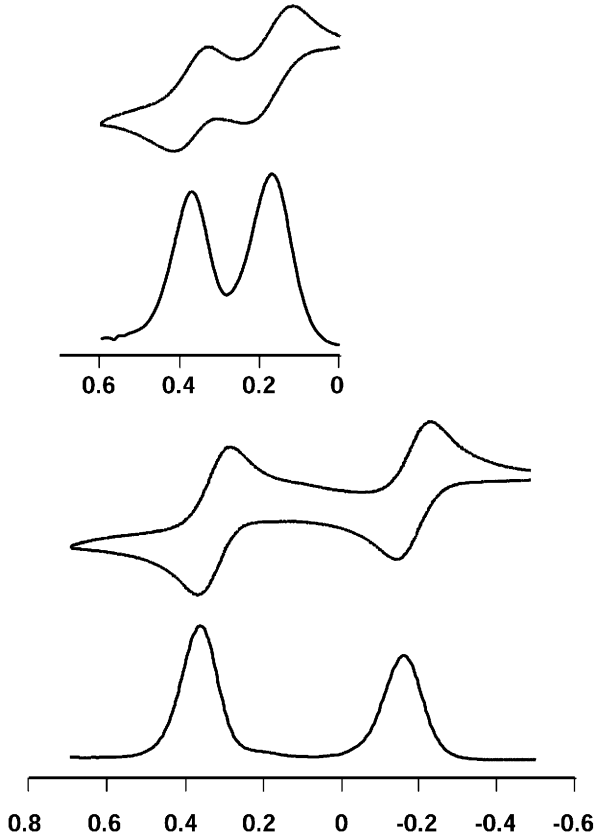

Figure 5. Cyclic voltammograms (CV) and differential pulse voltammograms (DPV) for α [Mo_2(DAniF)$_3$]$_2$(*N*,*N*′-di-*p*-anisyloxamidate), **3** (upper), and *β* [Mo_2(DAniF)$_3$]$_2$(*N*,*N*′-di-*p*-anisyloxamidate), **5** (lower). The electrochemical behavior of **2** and **4** are similar to those of **3** and **5**, respectively. Note that the *β* isomers have a much larger $\Delta E_{1/2}$. The potentials are given in volts versus Ag/AgCl.

One is the electrostatic repulsion between the two charged centers, [Mo_2^{5+}]L[Mo_2^{5+}] in our case, which will tend to destabilize the doubly charged species, and the other is the stabilizing effect of electron delocalization over the two dimetal centers, which is expected for the mixed-valence species, [Mo_2^{5+}]L[Mo_2^{4+}] in this case. Systematic studies on various dicarboxylate-linked dimolybdenum pairs have shown that saturated dicarboxylate groups hinder communication but involvement of conjugated linkers enhances the electrochemical and electronic communication.[4a,41]

While, as just noted, it is qualitatively understood that the electronic communication between two linked redox sites is dependent on the nature of the linker, there is interest in evaluating the two major contributors, electrostatic interactions and electronic delocalization, in a more quantitative manner.[41,44b,45] This is important because such studies extend our knowledge of intramolecular electron-transfer processes. The appearance of two geometric or linkage isomers resulting from different coordination modes, as reported here, offers an unusual opportunity to achieve additional understanding.

On the basis of the results of electrochemical measurements, the two [Mo_2] centers in **2** and **3** are only moderately coupled by the orthogonal oxamidate. The values of $\Delta E_{1/2}$ (ca.190 mV) and the magnitudes of K_c (10^3) are comparable to those for the compounds with tetrahedral linkers.[9,10] A common structural feature in these compounds is that the two [Mo_2] units are

(45) Sutton, J. E.; Taube, H. *Inorg. Chem.* **1981**, *20*, 3125.

Scheme 4

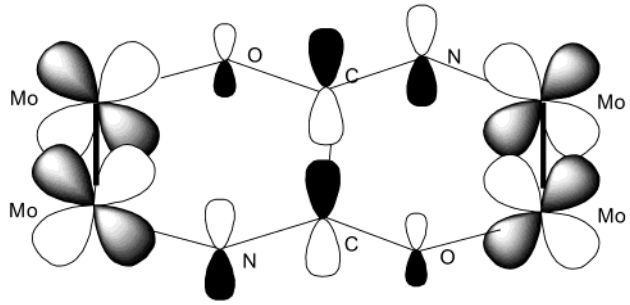

perpendicular to one another. With this geometry, electronic delocalization via metal−ligand back-bonding ($\delta \rightarrow \pi^*$) is minimized. Electrostatic interactions between the two dimetal centers are significant due to the relatively short Mo_2−Mo_2 distances (6.45−7.12 Å) and are presumably the major contributor to the value of $\Delta E_{1/2}$ (or K_c).[9,10] Therefore, these compounds may be assigned at best to Class II, in terms of the Robin−Day classification.[46] For the oxalate analogue, which has a slightly higher $\Delta E_{1/2}$ of 212 mV (K_c of ca. 10^3), the electrostatic interaction may be supplemented by electron delocalization arising for the oxalate analogue because of the planar configuration. The greater Lewis basicity for oxamidate would be expected to affect the potentials ($E_{1/2}$) of individual redox processes but not necessarily the difference, $\Delta E_{1/2}$.

By comparison with the α isomers, the *β* isomers **4** and **5** display a remarkably large potential separation ($\Delta E_{1/2}$) for the two one-electron oxidation processes, from which a K_c of 10^9 is derived; therefore, the mixed-valence compounds of this system appear to belong to Class III ($K_c > 10^6$), which is dominated by electron delocalization. These are the most electronically delocalized compounds having dimetal units that have been structurally characterized.[47] The electronic coupling effect is greater than that observed in the Creutz−Taube complex, pyrazine-bridged decaammineruthenium ion, for which a K_c of 3.6×10^6 derived from the $\Delta E_{1/2}$ of 390 mV [48,49] is 3 orders of magnitude smaller than the K_cs for **4** and **5**.

The large electronic delocalization implies that (1) in the mixed-valence species {[Mo_2]L[Mo_2]}$^+$ the unpaired electron is distributed over the two [Mo_2] centers, as is the charge; (2) there are extensive metal−metal interactions between the two [Mo_2] units; (3) in solution, the singly oxidized species {[Mo_2]L[Mo_2]}$^+$ is thermodynamically stable toward disproportionation. It is fairly obvious that the exceptional electrochemical behavior observed for **4** and **5** must be attributed to their unusual molecular structure, specifically, the *β* coordination mode of the oxamidate. As discussed earlier, in the *β* isomers the two [Mo_2] units and the oxamidate linker are constrained within two fused, rigid six-membered rings. With this geometry and symmetry, the *δ* orbitals of the [Mo_2] units efficiently interact with the π^* orbital of the oxamidate; as a result $\delta \rightarrow \pi^*$ back-bonding from the dimetal units to the linker is maximized (Scheme 4). It is understandable that the electron delocalization over such *π* systems is facile and efficient. The

(46) Robin, M.; Day, P. *Adv. Inorg. Chem. Radiochem.* **1967**, *10*, 247.
(47) A compound with a similar K_c is [(DAniF)$_2$$Mo_2$]$_2$(*μ*-Cl)$_4$. See: Cotton, F. A.; Liu, C. Y.; Murillo, C. A.; Wang, X. *Chem. Commun.* **2003**, 2190.
(48) Creutz, C.; Taube, H. *J. Am. Chem. Soc.* **1973**, *95*, 1086.
(49) Demadis, K. D.; Hartshorn, C. M.; Meyer, T. J. *Chem. Rev.* **2001**, *101*, 2655.

linkage of the oxamidate anions makes these compounds significantly different from the oxalate analogue in the extent of electron delocalization, even though a $\delta \rightarrow \pi^*$ transition is observed in the oxalate-linked compound.

Near-IR Spectra of the Singly-Oxidized α and *β* Forms. Further support for the large impact by the linker binding mode in modifying electronic communication is provided by a comparison of the near-IR spectra of the oxidized products of the α and *β* forms. Oxidation of both the α and *β* isomers was accomplished by addition of 1 equiv of ferrocenium hexafluorophosphate to CH_2Cl_2 solutions of the corresponding isomer. The near-IR spectra were measured immediately after oxidation had occurred by taking an aliquot of the reaction mixture (a ferrocene solution in dichloromethane did not absorb in the 800 to 3000 nm region.)

Each cation, $\mathbf{4}^+$ and $\mathbf{5}^+$, shows a relatively intense band centered at 4739 and 4695 cm^{-1}, respectively, which can be assigned as what is conventionally called an intervalence charge-transfer band.[44,49] The corresponding molar absorptivities and bandwidths are 2.1×10^4 and 2.0×10^4 M^{-1} cm^{-1}, and 1186 and 1130 cm^{-1}. For $\mathbf{2}^+$ and $\mathbf{3}^+$ the near-IR spectra do not show such absorptions. This is consistent with a significant increase of the electronic communication in shifting from the α binding mode to the *β* binding mode.

A more quantitative measure of the degree of communication can be obtained by using the Hush formula $\Delta\bar{\nu}_{1/2} = [2310(\bar{\nu}_{max})]^{1/2}$ which holds for Class II mixed-valence species, but not for Class III compounds for which the experimental bandwidth at half-height, $\Delta\bar{\nu}_{1/2}$, tends to be less than what this equation suggests.[50] Using the values for $\mathbf{4}^+$ and $\mathbf{5}^+$, the calculated values for $\Delta\bar{\nu}_{1/2}$ of 1750 and 1610 cm^{-1}, respectively, are larger than the experimental values. This suggests that the *β* isomers should be classified above Class II, possibly in the Class III category, as suggested by the electrochemical measurements mentioned earlier. A definite classification will have to await further studies of other $[Mo_2]$linker$[Mo_2]$ compounds. The lack of intervalence charge-transfer bands in the α monocations suggests that they should be viewed as belonging to Class I.

Molecular Mechanics Calculations. In the α isomers the C−C bond of the oxamidate bridging ligand is a single bond and the two $[Mo_2]$ units are in principle free to rotate. Why in these compounds are the torsion angles close to 90° in contrast with that of the oxalate analogue, which has a planar structure? For the α-oxamidate-bridged compounds, planar structures that could be either *cis* or *trans* may be considered. The *cis* conformation is not feasible because it would require that the two phenyl groups on the bridging oxamidate N atoms be side by side. We can therefore refer the twist angle between the two $[Mo_2]$ units in an α isomer to the *trans* planar form with an angle of 0°. Theoretical work by Bursten and Chisholm for oxalate-linked compounds having $M_2(O_2CR)_3$ units (M = Mo and W) favored the pseudo planar D_{2h} configuration, but only by a few kJ mol^{-1}.[33b] It should be noted that theoretical calculations for the isolated oxalate anion show a small energy difference between rotamers, and the conformation in D_{2d} symmetry instead of the planar D_{2h} is slightly favored.[17]

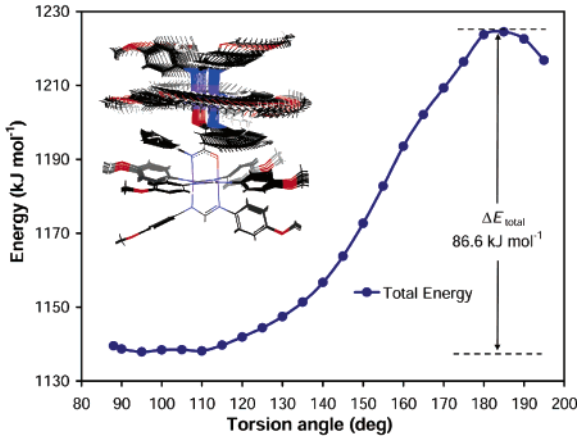

Figure 6. Variation of the minimized energy versus O−C−C−O angle for $[Mo_2](ON(Ph)C-CN(Ph)O)[Mo_2]$. The inset shows the conformational changes of the molecule at various torsion angles.

Molecular mechanics (MM) calculations were performed on the phenyl-substituted oxamidate compound to evaluate the effect of steric interactions, with the starting geometry being adopted from the single-crystal structure of **3**. The internal twist of the two $[Mo_2]$ units along the C−C bond is defined by the torsion angle of O−C−C−O in the bridging oxamidate ligand as shown in IX. Minimization of total energy was carried out by fixing the geometry of the $[N_6Mo_2](ON(Ar)C-CN(Ar)O)-[Mo_2N_6]$ core and then varying the torsion angle defined by the O−C−C−O group from 85 to 195° in 5° increments. At each step, all six anisyl groups from the formamidinate ligands and the aryl groups on the oxamidate bridge were unrestrained and they were allowed to rotate until the energy minimization converged. A plot of minimized total energy at each calculated torsion angle is shown in Figure 6. The results show that the gauche conformation with a twist angle at about 90° is preferred over the planar structure by 86.6 kJ mol^{-1}. The increase of energy in going from the gauche to planar structure is mostly due to greater steric repulsions found at smaller twist angles. The simulation indicates that the phenyl groups on the oxamidate bridge must rotate ca. 47° around the C_{aryl}−N bond and open the C−N−C_{aryl} angle by 5° to accommodate the change from the gauche structure to planar. In addition, conformational changes of the formamidinate ligands are required to minimize the close contact between formamidinate anisyl groups and oxamidate phenyl groups (see inset in Figure 6). The result is consistent with the observed single-crystal structures.

DFT Calculations. A series of Density Functional Theory (DFT) calculations were done to gain more insight into the effect of both the steric and electronic interactions on the stability of the α isomers. A calculation was also performed on the *β* isomer for comparison. These were carried out on model compounds of the form $[(HNC(H)NH)_3Mo_2]_2ON(R)C-CN(R)O$ where the aryl groups of the formamidinate groups were replaced by hydrogen atoms and the oxamidate substituents were either hydrogen atoms or phenyl groups. For comparison we also did calculations on the free and isolated oxamidate dianion.

A DFT geometry optimization of the $[ON(H)C-CN(H)O]^{2-}$ shows that the species with C_{2h} symmetry represents the potential minimum. Thus, the free oxamidate dianion with R = H prefers the planar conformation. To further compare the energy difference between the planar C_{2h} and the gauche C_2 structures of the oxamidate ion, the OC−CO torsion angle was

(50) See for example: (a) Hush, N. S. *Coord. Chem. Rev*. **1985**, *64*, 135. (b) Laye, R. H.; Couchmann, S. M.; Ward, M. D. *Inorg. Chem*. **2001**, *40*, 4089. (c) Scheiring, T.; Kaim, W., Olabe, J. A.; Parise, A. R.; Fiedler, J. *Inorg. Chim. Acta* **2000**, *300*−*302*, 125.

Table 4. Results from DFT Calculations

model	substituent[a]	constrained OCCO torsion angle (deg)	energy (a.u.)	calculated bond lengths, Å: Mo–Mo	calculated bond lengths, Å: C–C
α isomer	H	180	−1504.297688	2.1419	1.4967
	H	90	−1504.279101	2.1392	1.5161
			Δ −48.79 kJ mol^{-1}		
	Ph	180	−1966.294996	2.1389	1.5024
	Ph	90	−1966.296150	2.1375	1.5207
			Δ 3.03 kJ mol^{-1}	2.0927(8)[b]	1.50(1)[b]
β isomer			−1966.295626	2.1388	1.5127
				2.0945(4)[c]	1.526(6)[c]

[a] Substituents on oxamidate groups; [b] Experimentally observed distance for **3**. [c] Experimentally observed distance for **5**.

Scheme 5

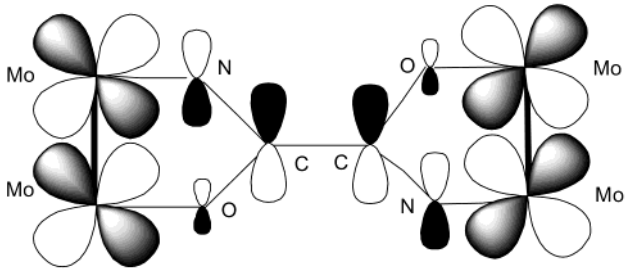

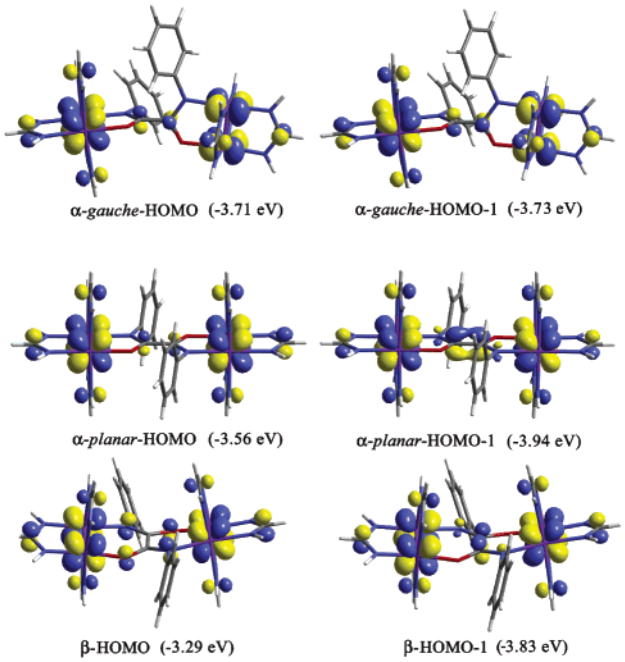

Figure 7. Illustration of the 0.04 contour surface diagrams from the DFT-calculated HOMOs and HOMO-1s for the R = Ph models.

constrained to 90° and the geometry was optimized under C_2 symmetry. The resulting geometry is 0.37 eV (35 kJ mol^{-1}) higher in energy than the potential minimum. The 90° gauche structure corresponds to a transition state since it has only one imaginary frequency of 72.0i cm^{-1} that corresponds to hindered rotation about the C−C bond.[17b] This contrasts with the results of calculations on the free oxalate ion, which showed a slight preference for the nonplanar conformation.[17]

The [Mo_2] units were then included in the calculations with the aim of obtaining a quantitative measure of the electronic energy difference between the 90° gauche and the planar structures of the oxamidate-bridged model compounds. Two sets of DFT calculations on the models having R = H were performed. In one the OC−CO torsion angle in the oxamidate bridge was constrained to 90° and in the other this angle was 180°. The rest of the molecule was allowed to relax without constraints. As shown in Table 4, the energy difference, ΔE, between the gauche and planar structure for the model α isomers, is 48.77 kJ mol^{-1}. This difference is 12.8 kJ mol^{-1} larger than the rotation energy calculated for the free oxamidate ion. Because the steric interactions are minimal with R = H, it is likely that this energy difference is caused mainly by electronic effects due to the better interaction of metal and ligand orbitals in the planar structure. In the planar conformation there is mixing of the occupied δ orbital and empty ligand π^* orbital which stabilizes the structure. This is expected from the molecular orbital analysis by group theory as shown in Scheme 5.

To measure the contribution of the steric interactions in the α isomer model, the substituent R = H in the oxamidate group was replaced with a bulkier R = Ph group in the DFT calculation. A geometry optimization gave a gauche structure with a torsion angle close to 90°, independently of whether the starting geometry was planar or gauche. To further compare the energy difference between the gauche and planar structures, the OC−CO torsion angle of the oxamidate bridge was constrained to 90° and 180°, respectively, and each of the models was allowed to relax. In this case, the planar conformation found in the isolated oxamidate anion is no longer the potential minimum. Instead, the gauche conformation is the more stable structure although the energy difference between the two models (3.0 kJ mol^{-1}) is within computational uncertainty. If we assume that the phenyl groups do not significantly affect the electronic structure of the model, as is seen by the lack of participation of the phenyl groups in bonding orbitals (Figure 7), then the steric interactions due to the substitution of the oxamidate R groups from hydrogen to phenyl can be estimated as the sum of the ΔE values obtained from the model where R= H and R = Ph, or 51.79 kJ mol^{-1}. However, for **2** and **3**, the steric interactions are expected to be much larger, since the aryl groups of the formamidate ligands do in fact interact with the aryl group on the oxoamidate bridge as shown by the molecular mechanics simulations.

Molecular orbital analysis of the R = Ph model indicates that the HOMO and HOMO-1 in the α gauche isomer are very close in energy and they are similar in shape, as shown in Figure 7. In these frontier orbitals the two dimolydenum units are basically isolated from each other, with little ligand bridge character.[51] Thus, electronic communication between the two Mo_2 units is probably unimportant, which is consistent with the electrochemical data.

For comparison between the α and *β* isomers, a DFT geometry optimization of an oxamidate-bridged model *β* isomer where R = Ph was performed. The geometry of the model compound was allowed to relax without constraints. The resulting geometry closely resembled that found in the crystal structures of **4** and **5**, which show a small dihedral angle between the two Mo_2 units. Interestingly, the energy difference between the α and *β* model isomers is very small, with the α isomer being favored by only 13.8 kJ mol^{-1}. Such a small energy

(51) Bridge ligand to metal relative contribution: HOMO, 7.7%; HOMO-1, 7.1%.

difference is consistent with the experimental isolation of the two types of isomers.

Molecular orbital analysis from DFT calculations provides valuable information on the electronic difference between the two isomers. Contrary to what was found for the α isomers, manifest communication between the two dimetal units in the β isomer can be inferred from the frontier orbitals. It is significant that the HOMO-1 shows the δ to pπ* back-bonding interaction as depicted in Scheme 5, and discussed above, where a filled δ orbital donates electron density to the empty ligand π* orbital. Also, significant ligand character is observed in the HOMO.[52] This allows for electron delocalization between the two dimetal units, as observed experimentally. These results are also consistent with previous calculations by the Chisholm and Bursten groups on Mo_2 units bridged by oxalate anions.[33b] It is also worth noting that these results imply that by varying the torsion angle on the bridge, the electronic communication between the dimetal units can be controlled to some extent.

We also carried out time-dependent DFT (TD-DFT) calculations on the α and β isomers using the optimized geometry of the R = Ph model compound. Such TD-DFT calculations have proven useful in understanding the electronic spectra of compounds having two [Mo_2] units linked by dicarboxylate groups.[41] For the α isomer, the weak low-energy absorption band, experimentally observed at 436 nm and assigned to the $\delta \rightarrow \delta^*$ transitions, is calculated at 456 nm. This calculated excited state is composed of a transition originated from the HOMO to an unoccupied molecular orbital that has mainly δ* character in the metal atoms. This suggests that the two dimetal units are indeed independent of each other and behave as two separate units in the α isomers. For the β model, the calculation estimates a relatively intense transition at 580 nm, and a relative weaker one at 492 nm, in accord with the experimentally observed bands at 541 and 461 nm. The higher energy transition is essentially $\delta \rightarrow \delta^*$ in nature, as described in the spectroscopy section. The low-energy band is a HOMO → LUMO transition, which is basically an intense $\delta \rightarrow \pi^*$ (MLCT) transition. The LUMO has a significant amount of phenyl character due to the aryl groups in the oxamidate linkers, which enhances the intensity of this transition and gives the compounds their deep color.

Synthetic Considerations. In our laboratory, we have developed a general method of preparation of [Mo_2]L[Mo_2] compounds for L = dicarboxylate anions that consists of replacement of highly labile CH_3CN molecules from the cationic species $[Mo_2(DAniF)_3(NCCH_3)_2]^+$ by reaction with tetraalkylamonium dicarboxylate salts. In this way more than 20 compounds have been made in good yields and high purity. The method is applicable also to L = EO_4^{2-}, where E = S, Mo, and W. However, it fails in the synthesis of diamidate compounds because preparation of tetraalkylamonium salts of the oxamidates could not be accomplished and the use of stronger deprotonating agents such as alkyllithium reagents did not give isolable products. Therefore, we were forced to find an alternative route that consists of using sodium methoxide as deprotonating agent, but we have found that the reaction only worked optimally when excess methoxide is present in the reaction mixture. This puzzling observation can now be explained and has led to the development of a new precursor for diamidate-bridged Mo_2 units in which the starting material is the new compound $Mo_2(DAniF)_3(CH_3COO)$, **1**, which has a labile acetate group that is easily replaced while leaving the less labile formamidinate groups untouched.

To understand the present synthesis, it is necessary to understand the previous synthetic procedures. For the preparation of dicarboxylate-bridged units, the acetonitrile derivative $[Mo_2(DAniF)_3(NCCH_3)_2]^+$ is prepared by reducing $Mo_2(DAniF)_3Cl_2$ in acetonitrile using zinc metal and using this intermediate in situ, with the counterion being $ZnCl_4^{2-}$. This substance is separated from the excess zinc by filtration and $(Bu^n{}_4N)O_2CXCO_2(NBu^n{}_4)$ is added to make the final product.

With the aim of understanding what goes on with the synthesis of diamidates using an excess of sodium methoxide, we recently looked at the reaction of $[Mo_2(DAniF)_3(NCCH_3)_2]_2ZnCl_4$ with $NaOCH_3$ in the absence of diamidate and found that the product has two [Mo_2] units bridged by an unusual $Zn(OCH_3)_4^{2-}$ unit, namely, $[Mo_2(DAniF)_3]_2Zn(OCH_3)_4$.[10] This appears to be a necessary intermediate in the preparation of diamidate-bridged tetranuclear species. Of course, the question remains as to why the reaction with Li salts of the diamidates failed to give isolable compounds. The answer to this lies in the well-known fact that the amidates are significantly more basic than carboxylate groups and that coordinated CH_3CN and other nitrile molecules are activated by transition metals.[53] Examples are those where acetonitrile reacts by nucleophilic attack of water to generate amidates. Indeed, the first diamidate complex bound to dimetal units was prepared serendipitously by hydrolysis.[54] However, this is not a general method.

Thus, it appears that nucleophilic attack on the acetonitrile molecules in $[Mo_2(DAniF)_3(NCCH_3)_2]^+$ by the lithium salts of the diamidate anions is more rapid than formation of the desired product. The necessity of removal of acetonitrile molecules has led to their replacement with acetate groups in **1**. However, instead of doing this directly, we have found that an easier way to prepare **1** is by direct reaction of $Mo_2(O_2CCH_3)_4$ with the sodium salt of the formamidinate according to eq 1. The

$$Mo_2(O_2CCH_3)_4 + 3HDAniF + 3NaOCH_3 \rightarrow Mo_2(DAniF)_3(O_2CCH_3) + 3NaO_2CCH_3 + 3CH_3OH \quad (1)$$

convenience of this one-pot reaction and the high yield of the product are additional advantages of this material. In this reaction, acetate anions are displaced by the more basic DAniF ligands; the strategy to ensure pure three-DAniF substituted product is to control carefully the stoichiometry of the reaction.

Since diamidate anions are stronger Lewis bases than acetate groups, **1** reacts readily to form diamidate-linked dimolybdenum compounds by displacement of the acetate groups in $Mo_2(DAniF)_3(O_2CCH_3)$ with anions made by reacting a diamide and $NaOCH_3$. The general procedure is described by eq 2.

(52) Bridge ligand to metal relative contribution: HOMO, 19%; HOMO-1, 13%.

(53) (a) Cotton, F. A.; Daniels, L. M.; Murillo, C. A.; Wang, X. *Polyhedron* **1998**, *17*, 2781. (b) Bauer, C. B.; Concolino, T. E.; Eglin, J. L.; Rogers, R. D.; Staples, R. J. *J. Chem. Soc., Dalton Trans.* **1998**, 2813. (c) Concolino, T. E.; Eglin, J. L.; Staples, R. J. *Polyhedron* **1999**, *18*, 915. (d) Nagao, H.; Hirano, T.; Tsuboya, N.; Shiota, S.; Mukaida, M.; Oi, T.; Yamasaki, M. *Inorg. Chem*. **2002**, *41*, 6267.

(54) Nelson, K. J.; McGaff, R. W.; Powell, D. R. *Inorg. Chim. Acta* **2000**, *304*, 130.

$$2Mo_2(DAniF)_3(O_2CCH_3) + RNHC(O)XC(O)NHR + 2NaOCH_3 \xrightarrow{THF} \xrightarrow[EtOH]{MeCN\ or} [Mo_2(DAniF)_3]_2[RNC(O)XC(O)NR] + 2NaO_2CCH_3 + 2CH_3OH \quad (2)$$

For the specific diaryloxamidate groups used in the present work, there are several additional important preparative aspects to be noted. First, the reaction described by eq 2 does not produce the final diamidate linked product in one step. Subsequent treatment of the reaction mixture with polar solvents is necessary for the formation of the product. Second, for a given linker, two isomeric forms, namely, α and β isomers, have been isolated. Third, the isomeric form obtained is dependent on the ways by which the solid from the reaction mixture is treated. A yellow α isomer (**2** or **3**) is produced immediately when the solid from the reaction mixture is treated with acetonitrile, whereas a dark-red β isomer (**4** or **5**), along with a considerable amount of the α isomer, is obtained after treatment with hot ethanol.

It is important to mention that we have found that both α and β isomeric forms are stable once formed and no conversions from one to the other have been observed by treating either one of them with acetonitrile or hot ethanol. This experimental observations favors the existence of a yet to be identified intermediate produced in the first step of eq 2 before the isomeric species are formed by treatment with various solvents. Evidently, this intermediate species is capable of undergoing different transformations depending on the reaction conditions. An extra driving force resulting in instant formation of the final products after addition of polar solvents is the insolubility of the neutral α and β forms in these solvents. Although mechanistic aspects of the reaction are still not clear, the experimental fact that heating is required to make the β isomers supports the idea that the α form is kinetically favored but it is not necessarily the thermodynamic product. Recognition of the steric effect resulting form the bulky aryl groups of the oxamide might be helpful in understanding the synthetic chemistry in this complex system. We are exploring this issue further by using smaller substituents as in *N*,*N*′-dimethyloxamidate. Preliminary results appear to indicate that the reaction proceeds neatly as described by eq 2, producing only the pure β analogue.[55]

Concluding Remarks

The isolation of two geometric isomers formed from the same linking ligand offers an unprecedented opportunity to study how the isomerization of a linking unit affects the molecular structure, electronic structure, and redox properties of the compounds with two [Mo_2] units which serve as redox sites. For these compounds, the two [Mo_2] centers are linked by a diaryloxamidate, which are structurally related to the oxalate ion, but both the α and β isomers are structurally different than the oxalate analogue. Considering the extent of the π orbital interactions of the dimetal units [Mo_2] (δ) with the linker (π), an increasing order is seen from the α species to the oxalate-linked analogue to the β species; the same order is presented in electronic coupling effects as measured by the $\Delta E_{1/2}$ for the series of compounds. By comparison, it is confirmed that electron delocalization, which is dependent on orbital overlap, is crucial to enhance the electronic communication. While the electron delocalization for the oxalate analogue makes a minor contribution to the $\Delta E_{1/2}$ (or K_c), the electron delocalization for the β form of oxamidate-linked compounds makes a great contribution.

Compounds **4** and **5** are particularly interesting not only because of the unusual coordination mode of the oxamidate ion to the dimetal units but more importantly because this type of structure has a major impact on the electronic structure and the redox properties associated with the two dimetal units. With this linkage mode, the electronic communication between the dimetal centers is greatly enhanced. According to the magnitudes of K_c (10^9), and the characteristics of the so-called intervalence charge-transfer band, the monocationic species could be classified as a Class III complex in terms of the Robin−Day classification. In comparison with other compounds having a M···M separation in the same range, for instance, the pyrazine-bridged diruthenium or Creutz−Taube complex, the electronic communication observed in this system is 3 orders of magnitude stronger. The intense, low-energy absorption band in the near-IR region of the electronic spectra can reasonably be assigned as the so-called intervalence charge-transfer band which supports strong orbital interaction between the metal units and the linker. This metal−metal interaction is facilitated through π interaction over the entire fused bicyclic chelating ring.

For such a system, in which a strong electronic communication occurs between two linked dimetal units, more interests lie on the singly and doubly oxidized compounds as more questions about the structural, magnetic, and spectroscopic aspects would be raised by these systems. We are planning to chemically oxidize and isolate compounds in the β mode and study these questions.

Acknowledgment. We thank Lisa Pérez for helpful discussions on the DFT calculations, the Laboratory for Molecular Simulation for software, and the Supercomputing Facility at Texas A&M University. We also thank the National Science Foundation, the Robert A. Welch Foundation, and Texas A&M University (through the Laboratory for Molecular Structure and Bonding) for financial support.

Supporting Information Available: A thermal ellipsoid plot of **1** (pdf) and X-ray crystallographic data (CIF) for **1**, **3**·$2CH_2Cl_2$, **4**·$2CH_2Cl_2$, and **5**·$2CH_2Cl_2$. This material is available free of charge at http://pubs.acs.org.

JA036884E

(55) Cotton, F. A.; Liu, C. Y.; Murillo, C. A., Villagrán, D.; Wang, X. Unpublished results.